ChemPhysChem

Chemistry Europe
European Chemical Societies Publishing

Accepted Article

Title: DNA Origami Based Assembly of Au@Ag Nanostar Dimer Nanoantennas for Label-Free Sensing of Pyocyanin

Authors: Tapasi Sen, Vishaldeep Kaur, Swati Tanwar, and Gagandeep Kaur

To be cited as: *ChemPhysChem* 10.1002/cphc.202000805

Link to VoR: https://doi.org/10.1002/cphc.202000805

WILEY-VCH

ARTICLE WILEY-VCH

DNA Origami Based Assembly of Au@Ag Nanostar Dimer Nanoantennas for Label-Free Sensing of Pyocyanin

Vishaldeep Kaur, ‡ Swati Tanwar,‡ Gagandeep Kaur, and Tapasi Sen*

V. Kaur, Dr. S. Tanwar, G. Kaur, Dr. T. Sen
Institute of Nano Science and Technology
Phase -10, Sector-64, Mohali, Punjab -160062, India
*E-mail: tapasi@inst.ac.in

[‡] Authors have contributed equally

Abstract: Early stage detection of diseases caused by pathogens is a prerequisite for expedient patient care. Due to the limited signal-to-noise ratio, molecular diagnostics needs molecular signal amplification after recognition of the target molecule. In this present study, we demonstrate the design of plasmonically coupled bimetallic Ag coated Au nanostar dimers with controlled nanogap using rectangular DNA origami. We further report the utility of the designed nanostar dimer structures as efficient SERS substrate for the ultrasensitive and label-free detection of the pyocyanin molecule, which is a biomarker of the opportunistic pathogenic bacteria, *Pseudomonas aeruginosa*. The experimental results showed that the detection limit of pyocyanin with such nanoantenna based biosensor was 335 pM, which is much lower than the clinical range of detection. Thus, fast, sensitive and label-free detection of pyocyanin at ultralow concentration in an infected human body can pave a facile route for early stage warning for severe bacterial infections.

1. Introduction

Highly sensitive, rapid and reliable detection of biomarkers is of utmost importance to improve early stage diagnosis and prevention of several bacterial infections and fatal diseases.[1] Molecular recognition of microbial biomarkers released by pathogens is highly required during early stage infection as it facilitates the early diagnosis of the onset diseases, monitoring their prognosis, and providing effective treatment.[2] One of the clinically important bacterial biomarkers requiring immediate attention in this direction is pyocyanin. It is a toxin uniquely released from Gram-negative bacterium *Pseudomonas aeruginosa* which is considered as one of the most problematic bacteria responsible for several infections.[3] Pyocyanin is assumed as a virulence factor as well as a quorum sensing signal for this microorganism which makes it an excellent biomarker for diagnosing the condition of a patient. Pyocyanin is involved in various important biological activities including gene expression, and is known to cause severe respiratory tract infections, especially in immunocompromised patients.[4] Therefore significant information about the presence of this pathogen and the state of progression of the infection in patients can be gained through the rapid and sensitive detection of pyocyanin in clinical samples.

Several biosensing techniques have been employed in the past for efficient detection of pyocyanin, such as high-performance liquid chromatography (HPLC) and Electrochemical sensing approaches.[5, 6] HPLC technique can quantify pyocyanin quite efficiently by recording its absorbance after solvent extraction, but involvement of expensive equipments and time-consuming procedures for pre-purification make it unfavorable for rapid detection of pyocyanin. Pyocyanin can also be directly quantified in clinical samples through electrochemical sensing in real time and in situ due to the redox-active nature of pyocyanin.[7] However, the selective quantification of pyocyanin is restricted by other redox-active molecules which are present in human fluids and by other metabolites released by pathogenic bacteria. Recently, Alatraktchi et al. demonstrated the fast selective identification of pyocyanin using cyclic voltammetry in clinically relevant concentration range of 2-100 µM.[8] In 2016, Sismaet et al. prepared a disposable screen printed electrode to detect pyocyanin in wound fluid from patients with chronic wounds.[9] However, false negative results in a complex mixture and lower sensitivity limit its practical applicability. Hence, in order to enhance the quality of life for millions by enabling the specific and rapid identification of analytes with high sensitivity, it is highly desirable to develop fast label-free sensing techniques to detect pyocyanin selectively in biological samples at ultra-low concentrations. Surface-enhanced Raman scattering (SERS) has recently emerged as a powerful analytical tool for the sensing of small molecules and biomolecules,[10, 11] by acquiring the Raman spectral signature of an analyte molecule of interest. The Raman spectrum of a molecule is a kind of fingerprint and the vibrational fingerprint of each molecule is unique which allows the identification and quantification of a molecule directly and specifically. Due to low Raman cross section of molecules, typically in the range of 10^{-25} - 10^{-30} cm^2 which is more than 10 orders of magnitude less than the fluorescence cross section, SERS technique has limited sensitivity.[12] Therefore signal enhancement through the electromagnetic field enhancement resulting from excitation of localized surface plasmon resonance (LSPR) of plasmonic nanostructures is essential for enabling SERS technique to detect analyte molecules at low concentration for broad applications ranging from chemical and bio-molecular sensing to food safety.

The unprecedented ability of SERS to detect a specific analyte from a complex mixture with extremely high sensitivity has fuelled the research in developing various SERS based sensing platforms[13, 14] using coupled plasmonic nanostructures as SERS substrates, such as dimers and trimers with ultrasmall nanojunctions (known as plasmonic nanoantennas)[15], where strong electromagnetic enhancement is observed due to extremely small hotspot region. Despite significant advances, SERS has shown limited feasibility for real-life applications, largely due to unachieved challenges in the substrate designing which includes gaining control over the nanogaps and precise localization of the analyte in the hotspot. Fang et al.[16] recently reported that out of 10^6 SERS active sites only 63 yields high enhancements indicating a rare occurrence of hotspots, so it is imperative to design new SERS active substrates that can yield high enhancement factors (EFs) with a narrow distribution and good reproducibility.

In recent years, the DNA origami technique has emerged as a powerful nanofabrication method for assembling nanoparticles into predesigned patterns with nanometer accuracy. Its ability to position biomolecules such as proteins,[17] DNAs,[18] and RNAs[19] at a predefined position allows localization of the analytes at the sensing region of the nanoantennas, difficult to achieve using high-end methods such as electron-beam lithography. This is a cost-effective alternative to the lithography technique, which otherwise poses a significant limitation in designing sub-nm resolution gaps.[20] Till now, DNA origami has led to a class of well-organized plasmonic nanoantennas such as Au nanoparticle dimers,[21, 22] bowtie nanoantenna,[23] and assembling Au nanolenses,[24] some of which have been used for concentration and manipulation of light into deep-subwavelength volumes.[21, 25] Our group has recently utilized rectangular DNA origami to construct Au nanostar dimers which were further used for single molecule SERS measurement of single Texas red dye molecule.[26] In another study, Heck et al. recently demonstrated SERS based detection of streptavidin protein molecule specifically positioned in the plasmonic hotspot of Ag nanolenses using triangular DNA origami.[27] The programmable nature of DNA origami allows it to be used as an engineering material for designing plasmonic based sensing devices.

So far, nanostructures of Au and Ag metals have been the most preferred choice for designing SERS substrates due to their unique and highly tunable plasmonic resonance properties from visible to near-infrared spectral range,[28] which directly translates into higher enhancements effects for molecules having electronic transitions in this region.[29] Over the past few years, bimetallic Au@Ag nanoparticles have come out as an excellent nanomaterial that displays interesting optical properties in comparison to their metallic counterparts due to the unification of properties of both the metals.[30] Comparative studies have shown that the SERS efficiency of Au@Ag bimetallic nanoparticles is higher than pure Au and Ag nanoparticles[31, 32] and has been attributed to a unique electronic transfer from the Au core to the Ag shell.[33] They also provide control over surface plasmon resonance (SPR) band tunability by simply changing the thickness of the Ag coating,[34] making them well suited for surface enhanced resonant Raman scattering studies (SERRS). It is well established that on-resonance measurements result in higher EFs than normal SERS.[35] In view of the multifunctional properties of bimetallic Au-Ag nanostructures, considerable efforts have been dedicated to explore their potential for SERS based applications.[36-38] In particular, anisotropic shaped nanostructures are of great interest owing to the presence of multiple intrinsic hotspots and broadly tunable plasmonic resonances.[28] To the best of our knowledge, there is no report in literature till date on formation of Au core- Ag shell nanostar dimer by using DNA origami technique.

Herein, we demonstrate the design of plasmonically coupled bimetallic Ag coated Au nanostar (Au@Ag NS) dimers with controlled nanogap using rectangular DNA origami. The designed nanoantennas exhibit superior plasmonic effects of Ag along with high chemical stability of Au. We have further demonstrated the utility of the designed nanoantennas as efficient SERS substrate for the ultrasensitive and label-free detection of bacterial biomarker, pyocyanin. The limit of detection of pyocyanin was found to be 335 pM, which is several orders less than the clinical range of detection (typically 7-130 µM).[39]

2. Results and Discussion

2.1 Synthesis and DNA functionalization of bimetallic Au@Ag NSs

Bimetallic Au@Ag NSs used in this study were synthesized by the epitaxial growth of Ag over preformed Au NSs as illustrated in figure 1a.[34] Similar lattice parameters (0.40786 nm for Au and 0.40862 nm for Ag) lead to epitaxial growth of Ag over Au NP core providing a high degree of control over shape and size of the nanoparticles and has been widely explored. [30, 40] During the synthesis of the Au@Ag NSs, the major challenge was to achieve a uniform coating of Ag over the previously synthesized Au NSs such that the sharpness of the tips remains unaltered. However, we were able to overcome the aforementioned challenge by precise control of the concentration of Ag in the coating solution. The Au NSs used for the synthesis were prepared according to our previously published report.[26] In the coating solution, $AgNO_3$ was the precursor of Ag and ascorbic acid was used as the reducing agent. The reduction of Ag^+ ions to Ag^0 by ascorbic acid was commenced on addition of NH_4OH solution, as evidenced by the change in color of the solution from blue to pinkish purple (Inset of Figure 1b). The redox potential of ascorbic acid is not sufficient to reduce Ag ions at low or neutral pH, hence, addition of NH_4OH immediately changed the pH of the reaction mixture to basic (pH~9) thereby initiating the reaction.[41] The overlapping UV-Visible absorption spectra of the Au NSs before and after Ag coating (Figure 1b) show a blue shifting of SPR band of Au NSs from 715 nm to 552 nm covering almost the entire visible region. The blue shift with no change in the shape of the spectrum indicated a successful coating of Ag over Au NSs with no change in the morphology. Further, from the TEM images of NSs (Figure 1c and 1d), it was evident that Ag is getting deposited on the surface of Au NSs and no separate nucleation is taking place. Due to significant similarity in the lattice fringe width of both the metals[42] Ag was deposited uniformly over the Au NSs leaving the sharpness of tips unaltered (as shown in Figure 1c and 1d). By the statistical analysis of 20 different structures, the average size of Au@Ag NSs (tip to tip distance of same NS) was determined to be 70 ± 5 nm and the thickness of the Ag shell was approximately 2.5 nm with an estimated error of ± 0.5 nm (Figure S1). The Ag coating thickness on Au NSs as monitored by TEM images and their plasmon maximum depicted by UV-Vis spectra were consistent with the previous reports on Au-Ag hybrid nanostructures.[34, 43, 44] It is important to note that electronic interactions between the Au core and Ag shell depend on the thickness of the Ag shell, lesser the thickness of Ag coating better is the stability and plasmonic enhancement effects of the Au@Ag bimetallic structure.[45] Very recently, Feng et al. found that an Ag shell thickness of 2.4 nm is optimum for getting the highest charge transfer effects and biocompatibility (both in vitro and in vivo).[46] Further, to ascertain the presence of Au and Ag in the synthesized Au@Ag NSs, energy dispersive X-ray (EDX) analysis of the nanostructures was done (as shown in Figure S2). The EDX spectrum showed characteristic peaks for both the metals in the bimetallic Au@Ag NSs.

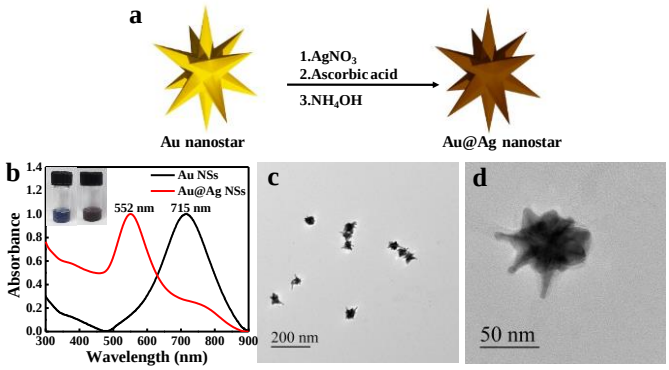

Figure 1. (a) Schematic depiction of the synthesis of Au@Ag NSs, (b) UV-Vis absorption spectra of Au NSs, and Au@Ag NSs (inset shows digital images of nanostar solutions), and (c and d) TEM images of Au@Ag NSs.

After the successful synthesis of the Au@Ag NSs, the next step was to functionalize the NSs with thiolated oligonucleotides. The DNA functionalization was carried out using the well-established method of salt aging with some modifications (Figure S3a). The initial step of attachment of thiolated DNA to Au@Ag NSs was carried out at pH 3 to overcome the problem of low adsorption of DNA on Ag surface at neutral pH.[47] Charge repulsion between phosphate backbones of adjacent DNA oligonucleotides was further reduced by increasing the salt concentration of solution very slowly to 750 mM. The UV-Vis spectra (Figure S3c) of Au@Ag NSs before and after DNA functionalization show a slight red shift of ~ 8 nm, which can be attributed to the change in the dielectric constant of surrounding medium after DNA conjugation.[48] During the immobilization of nanoparticles on DNA origami, buffer solutions having salt concentration as high as 500 mM NaCl were used. Hence, it was imperative to check the stability of the as-synthesized Au@Ag NSs in high salt concentration. We found that the DNA conjugated Au@Ag NSs solutions were able to withstand the salt concentration conditions required for immobilization on DNA origami (as shown in Figure S3a and S3b). The stability of Au@Ag NSs without DNA functionalization was also checked under different NaCl concentration and it was found that the absorption intensity dramatically reduced with the addition of 100mM NaCl and kept on decreasing with increase in the concentration of NaCl (Figure S4). This indicated that the synthesized Au@Ag NSs are highly unstable in high salt concentrations without DNA functionalization.

2.2 Assembly of Au@Ag NS dimers on DNA origami

After successful conjugation of synthesized Au@Ag NSs with DNA oligonucleotides, they were immobilized on rectangular DNA origami at a predefined position with the help of extended capturing DNA sequences.[26] The formation of DNA origami monomers and dimers was confirmed by agarose gel electrophoresis (represented in Figure S5), where clear bands corresponding to origami monomers and dimers were visible. The AFM and TEM images of dimerized rectangular DNA origami are depicted in figure S6 of the supporting information. For the construction of a plasmonically coupled Au@Ag dimer structure, two capturing sites were created, one on each monomeric unit of the dimerized DNA origami template. Each attachment site comprised of 5 capture sequences extended at 3' end with a sequence complementary to that of ssDNAs attached on Au@Ag NSs. The positions of the capturing DNA strands are given in table S1 of supporting information.[26] The Au@Ag NS dimer structures were synthesized as described in the experimental section. Preliminary structural characterization of the synthesized dimer structures was done using AFM imaging. AFM images and the corresponding height profile presented in Figure 2a confirmed the formation of dimer structures. TEM images confirmed that the dimer structures are forming with no change in the morphology of Au@Ag NSs after conjugation on the DNA origami template (Figure 2b and 2c). In case of Au nanostar dimer on origami, the origami template is faintly visible because the template probably got hidden behind the Au nanostar assemblies. The average size of single Au@Ag NSs (~70 nm) is comparable with the size of DNA origami monomer (~90 x 60 nm). However it was clearly visible in case of Au@Ag NSs monomer on DNA origami dimer (Figure S7). Furthermore, to obtain more insights into the elemental composition of the designed Au@Ag NS dimers, we characterized the designed nanoantenna using STEM-EDX mapping (shown in figure 2d, 2e and 2f). It showed that there was no change in the Ag coating after immobilization on DNA origami, suggesting that the coating is stable and is not getting removed during the DNA functionalization and assembly process. The EDX spectrum of Au@Ag NS dimers also showed peaks corresponding to phosphorus (P) and oxygen (O) along with Ag and Au, which is indicative of the presence of DNA on the nanostructures (Figure S8). The formation of desired nanostar dimer structures was prominent as evidenced from TEM images shown in Figure 1 and Figure S9. Since 2:1 ratio of Au@Ag NSs and DNA origami was used while immobilization, there was formation of monomers as well as trimers of Au@Ag NSs on DNA origami dimer along with other assemblies such as unbound origami, unbound Au@Ag NSs and few aggregated structures (Figure S9). Critical examination of the assembled structures revealed the formation of dimeric assemblies with high yield of 65% along with a few fractions of other assemblies on DNA origami (shown in Figure S10 and enlisted in Table S2) which was consistent with the previous report on assembly of nanoparticles dimer on DNA origami.[48].

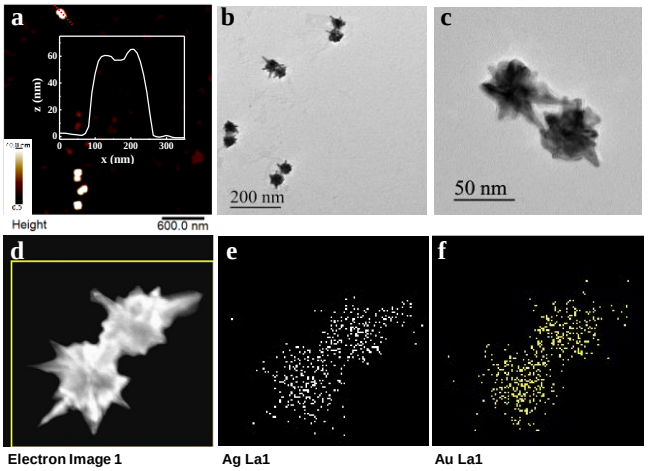

Figure 2. (a) AFM images of Au@Ag NS dimer structures (inset shows corresponding height profile), (b and c) TEM images of dimer structures of an average interparticle gap of 10 nm assembled on dimerized rectangular DNA origami, and (d) Dark field STEM mapping image of an Au@Ag NS dimer structure, and (e and f) the corresponding elemental mapping images.

The average interparticle gap (nanostar core to core distance) between the Au@Ag NS dimer structures was calculated by evaluating at least 20 different TEM images of the dimeric structures and was found to be 10 ± 1 nm (Figure S11). The tip to tip distances in the conjunction region that is present between tips and cores of two nanostars after considering several TEM images of nanostar dimer structures was also calculated and it was found to lie in the range of (~1 nm ≤ d ≤ 3.1 nm) as depicted in Figure S12.

2.3 Label-free SERS based detection of pyocyanin using Au@Ag NS dimer structures

After the successful synthesis and characterization of the designed nanoantenna, we have utilized our designed nanoantenna structures for label-free SERS-based detection of bacterial biomarker pyocyanin. The detection of pyocyanin was done using AFM correlated Raman measurements using a 633 nm laser excitation source for 1 second acquisition time (Figure 3). The AFM correlated Raman measurements were done using the similar procedure reported earlier.[26] For the measurements, at first, the assembled Au@Ag nanostar dimers were immobilized on Si wafer. The Si wafer was then scanned by AFM imaging for identification and localization of the features on the substrate. Later, the wafer was incubated with a drop of known concentration of pyocyanin (between 1 µM and 500 pM) to form a monolayer of pyocyanin over the Au@Ag NS dimers. The Raman spectra was then acquired by scanning the same area as depicted in AFM images identified by means of prominent features acting as marker on both the images. The SERS measurements were conducted by means of identification of a marker on Si wafer and then scanning the same area by confocal Raman microscope for capturing Raman signatures. During the measurements, the laser power was kept low (1 mW) so as to avoid any damage to the DNA origami template.

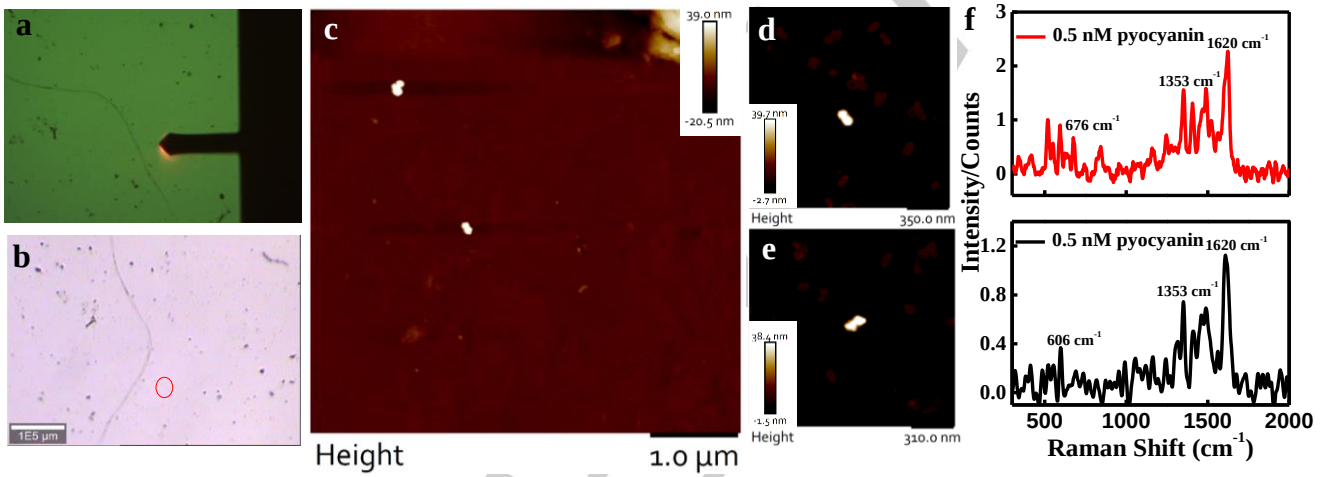

Figure 3. (a), and (b) Optical images captured using AFM and Raman microscope. (c) AFM image of Au@Ag NS dimers assembled on dimerized rectangular DNA origami, (d) and (e) High resolution AFM images of single Au@Ag NS dimeric structures, and (f) their corresponding SERS spectrum for pyocyanin.

Figure 4a illustrates the schematic depiction of the sensing of pyocyanin on Au@Ag NSs dimer nanoantennas. The UV-Vis absorption spectrum of pyocyanin shows a broad absorption band in the visible region (Figure 4b) with λ_{max} around 688 nm which is close to the laser excitation wavelength of 633 nm. Therefore, the Raman spectra recorded using the designed Au@Ag NS dimer nanoantennas were actually due to SERRS rather than SERS. Figure 4c shows the obtained concentration-dependent Raman spectra of pyocyanin. We were able to record detectable SERS signals over a concentration range of 1 µM to 500 pM with the intensities of the dominant peaks varying linearly with change in the concentration of pyocyanin. In order to identify the Raman signatures of pyocyanin and to ascertain that the recorded Raman signals are of pyocyanin only, we recorded the reference SERS spectrum of pyocyanin using 50 nm Ag nanoparticles (Figure 4d). The peaks in the reference spectrum matched well with the peaks obtained from our AFM correlated Raman measurements. The peak at 1357 cm^{-1} corresponds to the combined C-C stretch, C-N stretch, and C-H in plane bending modes of the aromatic ring.[49] The band around 1607 cm^{-1} is ascribed to the ring deformations and C-C stretching.[39]

Further, we confirmed that the recorded SERS signals were coming only from the pyocyanin molecules which are present on the Au@Ag NSs dimer nanoantennas. We have recorded normal Raman spectra of pyocyanin with varying the concentrations from 10 µM to 500 pM (shown in Figure S13). No characteristic Raman peaks were obtained for all the three concentrations of pyocyanin which proved that the intense SERS signal coming from pyocyanin molecules in the presence of Au@Ag NSs is due to the significant enhancement of the Raman signals by the hotspots of the nanoantennas. The appearance of the Raman signatures of pyocyanin molecules at 500 pM concentration confirms the suitability of Au@Ag NSs dimer structures on DNA origami as an excellent SERS substrate for detection of biomolecules at ultralow concentration. We had also performed the concentration dependent SERS measurements of pyocyanin in the junction of dimeric Au NSs assembled on DNA origami for comparison with Au@Ag NSs assembled dimeric structures (Figure S14). We were not able to

obtain the SERS spectra of pyocyanin below 10 nM concentration using Au NSs dimer on DNA origami. Furthermore, the SERS intensity corresponding to same pyocyanin concentration was lower in case of Au NSs dimers compared to Au@Ag NSs dimeric structures. Hence, better enhancement in Raman signals was observed due to Ag coating on Au NSs.

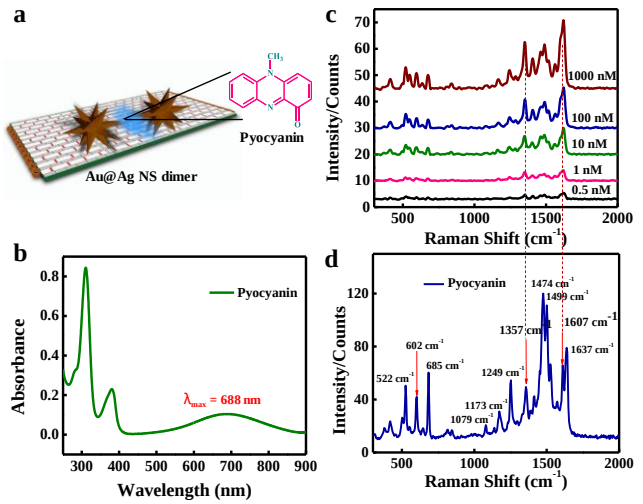

Figure 4. (a) Schematic depiction of pyocyanin sensing on the Au@Ag NSs dimer nanoantenna, (b) UV-Vis absorption spectrum of pyocyanin, (c) concentration-dependent SERS spectra of pyocyanin molecules placed on dimer nanoantennas, and (d) reference Raman spectrum of pyocyanin (1.5 mM) recorded on 50 nm Ag NPs.

Further, the limit of detection (LOD) was calculated according to well-known method of LOD estimation by International Union for Pure and Applied Chemistry (IUPAC) (Equation S1 of supplementary information).[50] The peak with the highest intensity at 1620 cm^{-1} in the obtained SERS spectra of pyocyanin was identified for the LOD calculation. The enlarged spectra around the highest peak intensity (1620 cm^{-1}) of the concentration dependent SERS plot of pyocyanin is depicted in Figure 5a and the relation between the concentration of pyocyanin and SERS intensity is shown by the scatter plot (Figure 5b). The average value of three repeated measurements for same concentration is depicted by each point on calibration curve, where the error bar represents the standard deviation. The plot clearly reveals a linear regime between the concentration and intensity, which can be expressed by relation,

$I_{1620} = 6.815 \times \log C + 3.714$ ($R^2 = 0.979$) Equation 1

where, I_{1620} is the SERS intensity at 1620 cm^{-1} and C is the corresponding concentration of pyocyanin in nM. By solving equation 1, the LOD of pyocyanin was determined to be 335 pM when pyocyanin was placed in the hotspot of Au@Ag NS dimer nanoantennas (Details in Supporting information).

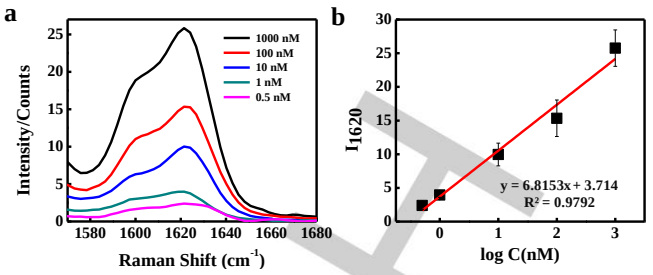

Figure 5. (a) SERS spectra monitored at 1620 cm^{-1} peak for different concentrations of pyocyanin, and (b) The SERS intensity at 1620 cm^{-1} as a function of pyocyanin concentration with linear fitting.

The obtained LOD was found to be lower than previously reported detection limit achieved using SERS and non-SERS based pyocyanin detection platforms.[39, 49, 51] For example, the detection limit of electrochemical sensor designed using palladium hydride electrode by Webster et al. was found to be 0.597 µM.[52] And that of Au/Ag nanoalloy modified thermoresistive polymer developed by Cernat et al. was 0.04 µM.[53] Recently, Jia et al. developed a biodegradable SERS platform using Au-coated zein film decorated with AuNPs and were able to achieve detection limit in micromolar range.[54] Nam et al. prepared monomeric Ag nanoarrays, which were directly self-assembled into anodized aluminium oxide (AAO) nanopores for SERS detection of pyocyanin upto 0.5 µM.[55] The array of $Au@SiO_2$ supercrystal developed by Bodelon et al. [56] and Au nanorods by Hanske et al.[57] yielded 10^{-14} M and 10^{-12} M sensitivity respectively, but the fabrication of such supercrystal and assembled SERS substrates required complex, expensive and time-consuming lithographic technique. In our case, we were able to get a sensitivity of 335 pM with a single Au@Ag dimer nanoantenna structure developed by using simple solution based technique. Table 1 depicts the comparative analysis of the LOD achieved using plasmonic sensor developed by our group with the previously reported ones. It clearly reveals that Au@Ag NS dimer nanoantenna self-assembled using DNA origami based approach offers a simple solution-based and biocompatible route for designing a highly sensitive pyocyanin detection platform, ruling out complex fabrication strategies and time-consuming techniques. We emphasize that the LOD can further be lowered and extended to other important biomarkers by specifically placing the analyte molecule by a target capturing probe molecule into the plasmonic hotspot.

Table 1. Comparison of different methods of pyocyanin detection

Material Used	Method Used	LOD	Reference
Ag NPs	SERS	500 nM	[39]
Zein/Au-Au NPs	SERS	25000 nM	[54]
Ag NP@AAO	SERS	500 nM	[55]
Au@SiO_2 supercrystal array	SERS	0.00001 nM	[56]
Au nanorods array	SERS	0.001 nM	[57]
Bimetallic Ag/Au NPs on Si nanowire	SERS	6250 nM	[58]
Pillar[5]ene stabilized Au NPs	SERS	100 nM	[51]
Ag nanorod array	SERS	23.8 nM	[49]
Au nanospheres	SERS	4.8 nM	[59]
Au and Ag electrodes	Cyclic voltammetry (CV)	2000 nM	[8]
Palladium hydride electrode	Square wave and differential pulse voltammetry	597 nM	[52]
Au/Ag nanoalloy modified electrodes	Electrochemical impedance spectroscopy (EIS)	40 nM	[53]
PANI/Au NPs/ITO modified electrodes	CV	500 nM	[60]
Carbon fibre two electrodes	Square wave voltammetry (SWV)	30 nM	[61]
Mixture of water-trifluoroacetic acid and acetonitrile-watertrifluoroacetic acid	HPLC	13 ng	[5]
Au@Ag NSs dimer nanoantenna	SERS	0.5 nM	Present paper

3. Conclusion

In summary, we have presented the design of bimetallic Au@Ag nanostars dimers assembled on DNA origami template. Bimetallic Au@Ag NSs were prepared by epitaxial growth of Ag over Au NSs that allowed extraordinary control over plasmon tunability and overall morphology of the nanostructures. The DNA origami substrates greatly facilitated a systematic route to model the nanostructures, arranging two 70 nm Au@Ag NSs on rectangular DNA origami with an average interparticle gap size of 10 nm. The designed dimer nanoantenna was utilized as a platform for SERS based label-free sensing of clinically important bacterial biomarker, pyocyanin. SERS spectrum clearly showed the distinguished bands assigned to pyocyanin at a concentration as low as 500 pM. It was found that our designed single dimeric assembly was able to detect pyocyanin with a limit of detection of 335 pM, which will aid in fast, label-free, and highly sensitive detection of pyocyanin and thus leading to rapid diagnosis of *P. aeruginosa* infections. Such DNA origami based self-assembled plasmonic nanosensors have the potentiality to open up new horizon in label-free detection of clinically important biomarkers with sensitivity down to single-molecule level.

Experimental Section

Materials

M13mp18 single stranded DNA was procured from New England Biolabs and was used without further purification. All the DNA oligonucleotides were purchased from Integrated DNA technologies (IDT) with HPLC purification. Gold chloride trihydrate ($HAuCl_4.3H_2O$, purity ≥ 99.9%), trisodium citrate dihydrate ($Na_3C_6H_5O_7$), L-Ascorbic acid, silver nitrate ($AgNO_3$), sodium dodecyl sulphate (SDS), tris-(carboxyethyl) phosphine hydrochloride (TCEP.HCl), Magnesium chloride hexahydrate ($MgCl_2.6H_2O$), pyocyanin, and sodium chloride (NaCl) were purchased from Sigma-Aldrich and used without further purification. Buffer solutions tris(hydroxymethyl)aminomethane (Tris base), 1 M potassium phosphate monobasic solution (KH_2PO_4), 1 M potassium phosphate dibasic solution (K_2HPO_4), ethylenediaminetetraacetic acid disodium (EDTA), HEPES buffer solution (pH-5) were purchased from Sigma Aldrich and used as received and Agarose was purchased from Himedia. Ammonium hydroxide (NH_4OH, 25%), hydrochloric acid (HCl), Tween 20, and acetic acid (CH_3COOH) were purchased from Merck. Sephacryl S-300 high resolution resin was bought from GE Healthcare. All the experiments were carried out in MilliQ water. Glasswares were thoroughly cleaned with aqua regia, water, and MilliQ water before using for experiments.

Synthesis of DNA origami

The rectangular DNA origami monomer was synthesized as previously described design proposed by Rothemund.[62] Briefly, M13mp18 scaffold was mixed with ~200 short staple strands and annealed in a PCR thermocycler followed by slow cooling using a 1.5 hour program. The folding was done using 10 fold excess staple sequences and 20 fold

excess modified staples in 1 × TAE buffer containing 12.5 mM $MgCl_2$ with scaffold concentration of 2 nM.

Rectangular DNA origami was dimerized as described in earlier report.[26] Briefly, two rectangular origami monomers were mixed with 40 fold excess of 24 branching staples in 50 × TAE buffer having 12.5mM $MgCl_2$. The solution was left undisturbed for 24 hours at room temperature to complete the process of dimerization. For further use, the excess unbound staples were removed by filtration using Sephacryl S-300 resin as described earlier.[26]

Synthesis of Au@Ag NSs

The Au nanostars (Au NSs) were synthesized using previously reported procedure.[26] To prepare Ag coated Au nanostars, 1 µL of 0.1 M $AgNO_3$, 1 µL of 0.1 M Ascorbic acid, and 1 µL of NH_4OH solution were subsequently added to 1 mL solution of Au NSs. Upon the addition of NH_4OH solution, the color of the solution changed from blue to purple indicating the coating of Ag on Au NSs. Then, 40 µL of 0.1 M SDS solution was added and the solution was kept on stirring for 10 minutes. Further, Au@Ag NSs solution was centrifuged at 4000 rcf for 10 minutes and the precipitate was redispersed in 5 mM HEPES buffer (pH 3).

Synthesis of DNA coated Au@Ag NSs

At first, disulfide protected DNA oligonucleotides were incubated with 200× molar excess of TCEP.HCl at room temperature for 3 hours. DNA functionalized Au@Ag NSs were then prepared using a modified fast pH assisted method as reported elsewhere.[47] Briefly, 1 mL solution of Au@Ag NSs dispersed in HEPES (pH 3) buffer was mixed with 5' thiol terminated deprotected DNA oligonucleotides with the DNA sequence: 5′-SH-CGTCGTATTCGATAGCTTAG-3′ followed by constant stirring for 1 hour. Then, 10% Tween 20 solution and 4:5 mixture solution of KH_2PO_4 and K_2HPO_4 buffers were added to the solution. After overnight incubation, stepwise addition of PBS solution having 2M NaCl and 0.1% Tween was done till the final concentration of NaCl reached 750 mM. The solution was further kept for overnight stirring at room temperature and purified by centrifugation followed by redispersion in 0.5 × TAE. The stability of resulting DNA-Au@Ag NS conjugates was determined using salt test.

Synthesis of DNA origami-Au@Ag NSs assemblies

The DNA conjugated Au@Ag NSs were hybridized with dimerized rectangular DNA origami by mixing in 2:1 molar ratio in 0.5 × TAE buffer with 300 mM NaCl. The mixed solution was kept in PCR and heated repeatedly between 20 °C and 40 °C for around 12 hours. Further, these assemblies were characterized using Atomic force microscopy (AFM) and Transmission electron microscopy (TEM) imaging.

UV-Visible spectroscopy

Ultraviolet-Visible (UV-Vis) absorption spectra of the synthesized Au, Au@Ag nanostructures and oligonucleotide modified Au@Ag NSs were recorded with a Shimadzu UV-2600 spectrophotometer.

TEM imaging

TEM imaging was done using a JEOL 2100 microscope at an accelerating voltage of 200 kV for Au@Ag NSs and 120 kV for DNA origami samples. For TEM imaging of Au@Ag NSs, sample was directly drop-casted onto carbon coated Cu grids followed by drying in a vacuum desiccator. The DNA origami samples were prepared by firstly activating the grid with 6 µL of $MgCl_2$ and then drop casting DNA origami sample (6 µL) on TEM grid. Negative staining was done using (2 % w/v) uranyl acetate solution. HAADF-STEM imaging of Au@Ag NS dimer on DNA origami was performed using JEOL, JEM-2100F microscope at an operating voltage of 200 kV equipped with EDX attachment.

AFM Imaging

AFM imaging was done using a Bruker Multimode 8 scanning probe microscope with TAP 150-Al-G cantilevers (Budget sensor). The AFM samples for DNA origami nanostructures were prepared on mica sheets of V1 quality. At first, freshly peeled mica surface was activated with 50 µM $MgCl_2$ solution for 10 minutes followed by washing with water and drying using N_2 gas. Then, 20 µL of purified origami dimer sample was drop casted onto the dried mica surface and incubated for 10 minutes. Further, the mica substrate was washed with MilliQ water followed by drying with N_2 gas.

To prepare AFM samples for Au@Ag NSs on DNA origami assemblies, 1 × 1 cm^2 Si wafers were plasma cleaned using Plasma bonder from Omicron scientific equipment Co. for 10 min to make the surface hydrophilic. The wafers were further cleaned with 1:1 solution of ethanol and MilliQ water and then incubated with dilute solution of sample in 10×TAE, 200mM $MgCl_2$ for approximately 2 hours. Afterwards, the wafer was washed excessively with MilliQ water to remove the unbound sample and further dried using N_2 gas.

Detection of pyocyanin using DNA origami-Au@Ag NSs assemblies

A stock solution of 1 mM pyocyanin was prepared by diluting the commercial pyocyanin solution in MilliQ water. Further, 10 fold diluted solutions were prepared by the subsequent dilutions of the stock solution. The Au@Ag NSs dimer sample was immobilized on Si wafer as described above and dimeric structures were identified using AFM. Further, 20 µL aliquot of different concentrations of pyocyanin solutions were drop-casted on Si wafer and wicked away after 30 minutes followed by drying with gentle breeze of N_2. By means of a scratch on Si wafer, the same area was scanned using Raman spectroscopy and the corresponding Raman spectra from the dimer structures were recorded using 633 nm laser (1mW) for 1 second acquisition time.

Author Contributions

‡These authors contributed equally.

Conflicts of interest

There are no conflicts to declare.

Acknowledgements

T.S. thanks Department of Science and Technology (DST) (SERB Project-ECR/2016/000436) for financial support. S.T. acknowledges INST for senior research fellowship. V.K. is thankful to DST-SERB project for providing junior research fellowship and INST for senior research fellowship. G.K. is thankful to INST for senior research fellowship. T.S. acknowledges IISER Kolkata TEM facility for STEM imaging.

Keywords: DNA origami, Au@Ag nanostars, Surface enhanced Raman spectroscopy, Pyocyanin, Plasmonic sensing

[1] S. Ghosh, N. I. Khan, J. G. Tsavalas, E. Song, *Front. Bioeng. Biotechnol.* **2018**, *6*, 29.
[2] Biomarkers Definitions Working Group, *Clin. Pharmacol. Ther.* **2001**, *69*, 89-95.
[3] E. Faure, K. Kwong, D. Nguyen, *Front. Immunol.* **2018**, *9,* 2416.
[4] M. Rybtke, L. D. Hultqvist, M. Givskov, T. Tolker-Nielsen, *J. Mol. Biol.* **2015**, *427*, 3628-3645.
[5] R. O. Fernández, R. A. Pizarro, *J. Chromatogr. A* **1997**, *771*, 99-104.
[6] Y. Yang, Y. Y. Yu, Y. Z. Wang, C. L. Zhang, J. X. Wang, Z. Fang, H. Lv, J. J. Zhong, Y. C. Yong, *Biosens. Bioelectron.* **2017**, *98*, 338-344.
[7] H. J. Sismaet, A. J. Pinto, E. D. Goluch, *Biosens. Bioelectron.* **2017**, *97*, 65-69.
[8] F. A. Alatraktchi, S. B. Andersen, H. K. Johansen, S. Molin, W. E. Svendsen, *Sensors* **2016**, *16,* 408.
[9] H. J. Sismaet, A. Banerjee, S. McNish, Y. Choi, M. Torralba, S. Lucas, A. Chan, V. K. Shanmugam, E. D. Goluch, *Wound Repair Regen*. **2016**, *24*, 366-372.
[10] K. C. Bantz, A. F. Meyer, N. J. Wittenberg, H. Im, Ö. Kurtuluş, S. H. Lee, N. C. Lindquist, S. H. Oh, C. L. Haynes, *Phys. Chem. Chem. Phys.* **2011**, *13*, 11551-11567.
[11] S. Zeng, D. Baillargeat, H. P. Ho, K. T. Yong, *Chem. Soc. Rev.* **2014**, *43*, 3426-3452.
[12] K. Kneipp, H. Kneipp, H. G. Bohr in *Single-Molecule SERS Spectroscopy, Vol. 103* (Eds.: K. Kneipp, M. Moskovits, H. Kneipp), Springer, Berlin, Heidelberg, **2006**, pp.261-277.
[13] T. Vo-Dinh, *Sens. Actuators, B* **1995**, *29*, 183-189.
[14] L. J. Xu, Z. C. Lei, J. Li, C. Zong, C. J. Yang, B. Ren, *J. Am. Chem. Soc.* **2015**, *137*, 5149-5154.
[15] J. M. McMahon, S. Li, L. K. Ausman, G. C. Schatz, *J. Phys. Chem. C* **2012**, *116*, 1627-1637.
[16] Y. Fang, N. H. Seong, D. D. Dlott, *Science* **2008**, *321*, 388-392.
[17] B. Saccà, R. Meyer, M. Erkelenz, K. Kiko, A. Arndt, H. Schroeder, K. S. Rabe, C. M. Niemeyer, *Angew. Chem., Int. Ed*. **2010**, *49*, 9378-9383.
[18] A. Gietl, P. Holzmeister, D. Grohmann, P. Tinnefeld, *Nucleic Acids Res*. **2012**, *40*, e110.
[19] Y. Ke, S. Lindsay, Y. Chang, Y. Liu, H. Yan, *Science* **2008**, *319*, 180-183.
[20] J. Chao, Y. Lin, H. Liu, L. Wang, C. Fan, *Mater. Today* **2015**, *18*, 326-335.
[21] A. Puchkova, C. Vietz, E. Pibiri, B. Wünsch, M. Sanz Paz, G. P. Acuna, P. Tinnefeld, *Nano Lett*. **2015**, *15*, 8354-8359.
[22] J. Prinz, B. Schreiber, L. Olejko, J. Oertel, J. Rackwitz, A. Keller, I. Bald, *J. Phys. Chem. Lett.* **2013**, *4*, 4140-4145.
[23] P. Zhan, T. Wen, Z. G. Wang, Y. He, J. Shi, T. Wang, X. Liu, G. Lu, B. Ding, *Angew. Chem., Int. Ed*. **2018**, *57*, 2846-2850.
[24] C. Heck, J. Prinz, A. Dathe, V. Merk, O. Stranik, W. Fritzsche, J. Kneipp, I. Bald, *ACS Photonics* **2017**, *4*, 1123-1130.
[25] J. Prinz, C. Heck, L. Ellerik, V. Merk, I. Bald, *Nanoscale* **2016**, *8*, 5612-5620.
[26] S. Tanwar, K. K. Haldar, T. Sen, *J. Am. Chem. Soc*. **2017**, *139*, 17639-17648.
[27] C. Heck, Y. Kanehira, J. Kneipp, I. Bald, *Angew. Chem., Int. Ed*. **2018**, *57*, 7444-7447.
[28] J. Reguera, J. Langer, D. J. de Aberasturi, L. M. Liz-Marzán, *Chem. Soc. Rev*. **2017**, *46*, 3866-3885.
[29] G. Moula, R. F. Aroca, *Anal. Chem.* **2011**, *83*, 284-288.
[30] M. F. Cardinal, B. Rodríguez-González, R. A. Alvarez-Puebla, J. Pérez-Juste, L. M. Liz-Marzán, *J. Phys. Chem. C* **2010**, *114*, 10417-10423.
[31] R. G. Freeman, M. B. Hommer, K. C. Grabar, M. A. Jackson, M. J. Natan, *J. Phys. Chem.* **1996**, *100*, 718-724.
[32] M. Fan, F. J. Lai, H. L. Chou, W.T. Lu, B. J. Hwang, A. G. Brolo, *Chem. Sci*. **2013**, *4*, 509-515.
[33] S. Nishimura, A. T. N. Dao, D. Mott, K. Ebitani, S. Maenosono, *J. Phys. Chem. C* **2012**, *116*, 4511-4516.
[34] A. M. Fales, H. Yuan, T. Vo-Dinh, *J. Phys. Chem. C* **2014**, *118*, 3708-3715.
[35] D. Cunningham, R. E. Littleford, W. E. Smith, P. J. Lundahl, I. Khan, D. W. McComb, D. Graham, N. Laforest, *Faraday Discuss*. **2006**, *132*, 135-145.
[36] W. Zhang, J. Liu, W. Niu, H. Yan, X. Lu, B. Liu, *ACS Appl. Mater. Interfaces* **2018**, *10*, 14850-14856.
[37] S. K. Krishnan, R. Esparza, F. J. Flores-Ruiz, E. Padilla-Ortega, G. Luna-Bárcenas, I. C. Sanchez, U. Pal, *ACS Omega* **2018**, *3*, 12600-12608.
[38] K.K. Liu, S. Tadepalli, G. Kumari, P. Banerjee, L. Tian, P. K. Jain, S. Singamaneni, *J. Phys. Chem. C* **2016**, *120*, 16899-16906.
[39] O. Zukovskaja, I. J. Jahn, K. Weber, D. Cialla-May, J. Popp, *Sensors* **2017**, *17,* 1704.
[40] Y. Sun, Y. Xia, *Nano Lett.* **2003**, *3*, 1569-1572.
[41] S. Gómez-Graña, B. Goris, T. Altantzis, C. Fernández-López, E. Carbo-Argibay, A. Guerrero-Martínez, N. Almora, N. López, I. Pastoriza-Santos, J. Pérez-Juste, S. Bals, G. van Tendeloo, L. M. Liz-Marzán, *J. Phys. Chem. Lett.* **2013**, *4*, 2209-2216.
[42] B. Rodríguez-González, A. Burrows, M. Watanabe, C. J. Kiely, L. M. Liz Marzán, *J. Phys. Chem. Lett.* **2005**, *15*, 1755-1759.
[43] Y. Ran, P. Strobbia, V. Cupil-Garcia, T. Vo-Dinh, *Sens. Actuators, B* **2019**, *287*, 95-101.
[44] Y. Yang, J. Shi, G. Kawamura, M. Nogami, *Scr. Mater.* **2008**, *58*, 862-865.
[45] D. M. Mott, D. T. N. Anh, P. Singh, C. Shankar, S. Maenosono, *Adv. Colloid Interface Sci.* **2012**, *185*, 14-33.
[46] Y. Feng, G. Wang, Y. Chang, Y. Cheng, B. Sun, L. Wang, C. Chen, H. Zhang, *Nano Lett.* **2019**, *19*, 4478-4489.
[47] X. Zhang, M. R. Servos, J. Liu, *Chem. Commun.* **2012**, *48*, 10114-10116.
[48] V. V. Thacker, L. O. Herrmann, D. O. Sigle, T. Zhang, T. Liedl, J. J. Baumberg, U. F. Keyser, *Nat. Commun.* **2014**, *5*, 3448.
[49] X. Wu, J. Chen, X. Li, Y. Zhao, S. M. Zughaier, *Nanomedicine (N. Y., NY, U. S.)* **2014**, *10*, 1863-1870.
[50] J. MocÁK, I. Janiga, E. RÁBarovÁ, *Nova Biotechnol. Chim.* **2009**, *9,* 91-100.
[51] V. Montes-García, S. Rodal-Cedeira, M. J. Cordero-Ferradás, B. Gómez, L. García-Río, I. Pastoriza-Santos, J. Pérez-Juste, *Isr. J. Chem.* **2018**, *58*, 1251-1260.
[52] T. A. Webster, E. D. Goluch, *Lab Chip* **2012**, *12*, 5195-5201.
[53] A. Cernat, A. Canciu, M. Tertis, F. Graur, C. Cristea, *Anal. Bioanal. Chem.* **2019**, *411*, 3829-3838.
[54] F. Jia, E. Barber, H. Turasan, S. Seo, R. Dai, L. Liu, X. Li, A. K. Bhunia, J. L. Kokini, *J. Agric. Food Chem.* **2019**, *67*, 4603-4610.
[55] N. N. Nam, T. L. Bui, S. J. Son, S. W. Joo, *Adv. Funct. Mater.* **2019**, *29*, 1809146.
[56] G. Bodelón, V. Montes-García, V. López-Puente, E. H. Hill, C. Hamon, M. N. Sanz-Ortiz, S. Rodal-Cedeira, C. Costas, S. Celiksoy, I. Pérez-Juste, L. Scarabelli, A. La Porta, J. Pérez-Juste, I. Pastoriza-Santos, L. M. Liz-Marzán, *Nat. Mater.* **2016**, *15*, 1203-1211.
[57] C. Hanske, E. H. Hill, D. Vila-Liarte, G. González-Rubio, C. Matricardi, A. Mihi, L. M. Liz-Marzán, *ACS Appl. Mater. Interfaces* **2019**, *11*, 11763-11771.
[58] O. Žukovskaja, S. Agafilushkina, V. Sivakov, K. Weber, D. Cialla-May, L. Osminkina, J. Popp, *Talanta* **2019**, *202*, 171-177.
[59] C. Q. Nguyen, W. J. Thrift, A. Bhattacharjee, S. Ranjbar, T. Gallagher, M. Darvishzadeh-Varcheie, R. N. Sanderson, F. Capolino, K. Whiteson, P. Baldi, A. I. Hochbaum, R. Ragan, *ACS Appl. Mater. Interfaces* **2018**, *10*, 12364-12373.
[60] A. A. Elkhawaga, M. M. Khalifa, O. El-Badawy, M. A. Hassan, W. A. El-Said, *PloS one* **2019**, *14*, e0216438.
[61] D. Sharp, P. Gladstone, R. B. Smith, S. Forsythe, J. Davis, *Bioelectrochemistry* **2010**, *77*, 114-119.
[62] P. W. Rothemund, *Nature* **2006**, *440*, 297-302.

Entry for the Table of Contents

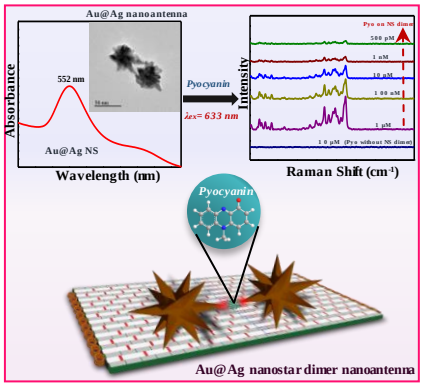

SERRS based detection of pyocyanin

The bimetallic plasmonic nanoantennas are a viable source to profoundly enhance the electromagnetic fields at the hotspot. Based on DNA origami nanofabrication route, this study demonstrate the ultrasensitive SERS based detection of bacterial biomarker pyocyanin using a single Au@Ag NS dimeric structure on DNA origami.